DHX15 as a novel immune-related prognostic biomarker in breast cancer: An integrated bioinformatics analysis with *in vitro* functional validation

FAN LI[1*], QIN YUE[2*] and JING LI[1,3]

[1]Department of Pathology, Tianjin Medical University General Hospital, Tianjin 300052, P.R. China;
[2]Department of Blood Transfusion, Tianjin First Central Hospital, Tianjin 300384, P.R. China;
[3]Department of Pathology, Tianjin Medical University, Tianjin 300070, P.R. China

Received March 18, 2026; Accepted July 17, 2026

DOI: 10.3892/ol.2026.15804

Abstract. Breast cancer (BC) is a disease that occurs relatively frequently, and its prognosis and treatment outcomes are not optimal at present. Identifying novel BC biomarkers and therapeutic targets is key. DEAH-box helicase 15 (DHX15) is an RNA helicase that exhibits enhanced activity and is closely associated with tumorigenic potential. Alternative splicing is widely dysregulated in BC. However, the biological function of DHX15 in BC, in addition to its underlying molecular mechanisms, remain unclear. DHX15, a key RNA helicase involved in splicing regulation, was therefore selected to explore whether it modulates the malignant progression of BC. The present study therefore analyzed the DHX15 expression profile in BC using the Tumor Immune Estimation Resource database. Kaplan-Meier plotter database was utilized to investigate the prognostic value of DHX15 in BC. The Cancer Genome Atlas-BRCA database was utilized to investigate the association between DHX15 and immune infiltration, as well as the expression of immune biomarkers, within the tumor microenvironment. The potential biological functions of DHX15 in BC were also investigated using Gene Ontology (GO) enrichment analysis, Kyoto encyclopedia of genes and genomes pathway analysis (KEGG) and single-cell functional analysis. GO and KEGG enrichment analyses were performed via the GSEA module embedded in the LinkedOmics database. Single-cell functional analysis was performed using the Human Proteome Atlas database and the CancerSEA database. Concurrently, the expression and function of DHX15 in BC was validated. MDA-MB-231 cells were transfected with a DHX15 knockdown plasmid and MCF-7 cells with an overexpression plasmid, and Transwell assays, plate cloning and scratch assays were performed on the established cell lines. The present findings revealed that the DHX15 expression levels in BC were notably higher compared with those in normal tissues. Furthermore, the expression of DHX15 was associated with immune checkpoints (such as PDCD1, LAG3 and GZMB) and immune cell infiltration (such as T helper cells and central memory T cells) in BC, as determined by single-sample Gene Set Enrichment Analysis and CIBERSORT analyses. *In vitro* experiments suggested that inhibiting DHX15 notably suppressed the migration, invasion and proliferation of MDA-MB-231 cells. Collectively, these findings suggest that the high expression of DHX15 in BC is associated with worse prognosis and immune cell infiltration, potentially by functionally promoting tumor cell proliferation, migration and invasion.

Correspondence to: Dr Jing Li, Department of Pathology, Tianjin Medical University, 22 Qixiangtai Road, Heping, Tianjin 300070, P.R. China
E-mail: lijing051789@tmu.edu.cn

*Contributed equally

Key words: DEAH-box helicase 15, breast cancer, biomarkers, immunotherapy targets, prognosis

Introduction

Breast cancer (BC) is the most prevalent malignant neoplasm among women. The most recent data from 2025 indicates that 32% of new cancer cases diagnosed in women are attributable to BC (1). BC can be classified based on molecular subtypes, namely luminal A, luminal B, HER2$^+$ and triple-negative BC (TNBC) (2). In the context of BC, the TNBC molecular type, characterized by the absence of the expression of estrogen receptor (ER), progesterone receptor and HER2, has been identified as a high-risk category with regard to the degrees of metastasis and recurrence (3). For early-stage BC, the primary treatment modality is typically breast-conserving surgery combined with radiation therapy (4). In the cohort of patients diagnosed with hormone receptor-positive cancer, endocrine therapy constitutes 80% of all treatment modalities. Nevertheless, not all patients respond positively to this therapeutic approach (1). The heterogeneity of BC presents notable therapeutic challenges. Nonetheless, progress in the fields of targeted therapy and immunotherapy has generated a renewed optimism regarding the management of the disease (5). The dynamic interaction between tumor progression and

immune microenvironment modulation serves a key role in BC development and therapeutic response (6). Therefore, it is imperative to conduct in-depth research into the mechanism of BC to discover novel biomarkers for providing novel targeted treatment options.

DEAH-box helicase 15 (DHX15) is a prominent member of the DEAD-box RNA-unwinding subfamily of the DEAD/H helicase family (7). DHX15 is traditionally recognized as an RNA unwinding enzyme that promotes mRNA maturation and ribosome assembly (7). However, studies have revealed multiple functions of DHX15 that were previously unknown. DHX15 deficiency in intestinal epithelial cells has been shown to increase tumorigenicity (8). In addition, DHX15 can fulfill a role in innate immunity through its capacity to act as a nucleic acid sensor. DHX15 has been reported to promote B cell survival and proliferation. Conditional knockout of DHX15 in B cells leads to B cell depletion and impaired humoral immune responses (9). DHX15 has also been identified as a regulator of natural killer (NK) cell homeostasis and function (10). Furthermore, DHX15 is involved in tumorigenesis, acting as an oncogenic driver in acute lymphoblastic leukemia, lung cancer, colorectal cancer and prostate cancer. By contrast, it has been documented to act as a tumor suppressor in glioma, hepatocellular carcinoma and gastric cancer (11-14). Previous studies have indicated that these helicases are essential for diverse cellular and physiological processes, including cell proliferation, hematopoiesis, inflammation, cancer pathogenesis, embryonic development and the regulation of autoimmune diseases (11-14). In addition, DEAD-Box helicase 5 and 17 play a role in transcriptional coactivation by interacting with transcription factors such as estrogen receptor α (ERα) and p53 in *in vitro* cellular models, which is involved in BC development (15). These molecules act as primary regulators of the estrogen signaling pathway by controlling transcription and splicing processes upstream and downstream of the ER (16). Therefore, a possible association exists between the therapeutic potential of targeting DHX15 in BC and its underlying tumorigenic functions. Nevertheless, the mechanisms of action, biological functions and regulatory patterns of DHX15 expression in BC remain to be fully elucidated.

The present study investigated the expression of DHX15 in BC and its effect on tumorigenesis, progression, development and prognosis. Moreover, the role of DHX15 in BC was examined by constructing a co-expression gene protein-protein interaction (PPI) network and performing pathway enrichment analysis to predict the underlying molecular mechanisms. Furthermore, the impact of DHX15 on tumor-infiltrating lymphocytes was analyzed. Finally, by downregulating DHX15 expression in MDA-MB-231 cells, knockdown efficiency was validated and the biological functions of DHX15 were assessed. The purpose of the present study is to reveal the potential diagnostic and prognostic value of DHX15 in BC, while also investigating its relationship with immune infiltration.

Materials and methods

Cell culture and reagents. Human BC MDA-MB-231 (cat. no. 240528I) and MCF-7 (cat. no. 20220817-01) cell lines were provided by Shanghai FuHeng Biotechnology Co. Ltd. All cells used in the present experimental procedure were cultured in DMEM (cat. no. KGL1206-500; Jiangsu KeyGen Biotech Co., Ltd.) supplemented with 10% FBS (Invitrogen; Thermo Fisher Scientific, Inc.) and 1% penicillin/streptomycin. Cells were incubated at 37˚C in a constant-temperature incubator with 5% CO_2.

Data download and analysis. The Cancer Genome Atlas (TCGA)-BRCA data, which consisted entirely of data on invasive breast cancer, were obtained from the publicly accessible Xena database (https://xenabrowser.net). Briefly, the cohort keyword TCGA Breast Cancer was used for retrieval, and the HTSeq-FPKM normalized RNA-seq expression dataset was selected. Tumor Immune Estimation Resource (TIMER1.0) (cistrome.shinyapps.io/timer) (17) was utilized for a comprehensive investigation of the molecular characterization of tumor-immune interactions. The 'Diff Exp' module was employed to investigate the differential expression of DHX15 between tumor tissue and adjacent normal tissue across all TCGA tumor samples; the paired normal tissues for TCGA-BRCA used in TIMER 1.0 were collected at least 2 cm from the tumor boundary, following the standard TCGA sample acquisition criteria, and verified as histologically normal tissue. For correlation analysis between DHX15 expression and immune cell abundance, the 'Gene' module was applied in the BRCA cohort, with purity adjustment and Spearman correlation calculation for six immune subsets (B cells, $CD8^+$ T cells, $CD4^+$ T cells, macrophages, neutrophils and dendritic cells). The 'Survival' module was used to explore the combined prognostic effect of DHX15 expression and immune infiltration by Cox regression analysis within TCGA-BRCA dataset. The University of Alabama at Birmingham Cancer (UALCAN) database (18) was utilized to validate the differential expression levels of DHX15 across distinct BC subtypes and its association with signaling pathways (http://ualcan.path.uab.edu). The Pathway Enrichment module of UALCAN was utilized to retrieve the top enriched biological signaling pathways significantly correlated with DHX15 expression in BC samples. The built-in statistical algorithm of UALCAN automatically calculated correlation coefficients and P-values for pathway enrichment.

Stable transfection using lentiviral infection. A 3rd generation lentiviral system was used to establish stable knockdown or overexpression cell lines. According to the manufacturer's instructions, 293T cells were used for lentivirus production, purification and subsequent infection (LentiPac™ HIV Expression Kit; GeneCopoeia, Inc). 293T cells were co-transfected with 2.5 μg of lentiviral expression plasmid and 2.5 μg of Lenti-Pac mixed packaging plasmid (containing packaging and envelope components) at 37˚C with 5% CO_2. At 48 h post-transfection, viral supernatants were collected, centrifuged (3,000 x g for 10 min at 4˚C) and filtered. Target cells were infected at a multiplicity of infection of 3. After 14 days of selection with puromycin (4 μg/ml) (cat. no. HY-B1743; MedChemExpress), stably transduced cells were maintained in medium containing the same antibiotic concentrations and used for subsequent experiments. The plasmids encoding DHX15 short hairpin RNAs (cat. no. HSH152517-LVRU6GP), an sh-control

(a non-targeting sequence) (cat. no. CSHCTR001-LVRU6GP), an overexpression plasmid (cat. no. EX-T8229-Lv122) and a control plasmid (cat. no. EX-NEG-Lv122) were provided by GeneCopoeia, Inc. The sequence of sh-DHX15 was as follows: Sense, 5'-CCGGGTGGAGTACATGCGATCATTACT CGAGTAATGATCGCATGTACTCCACTTTTTG-3' and antisense, 5'-AATTCAAAAAGTGGAGTACATGCGATC ATTACTCGAGTAATGATCGCATGTACTCCAC-3'. The sequence of sh-control was as follows: Sense, 5'-CCGGCG GCATGGACGAGCTGTACAATTTTTG-3'; and antisense, 5'- AATTCAAAAATTGTACAGCTCGTCCATGCCG-3'. Following transfection of 293T cells with the plasmids, the virus-containing supernatant culture was collected at 48 h post-transfection. At 48 h post-transfection, viral supernatants were collected, centrifuged (3,000 x g for 10 min at 4˚C) and filtered, and added to Polybrene. Polybrene can neutralize the electrostatic repulsion between the negatively charged lentiviral particles and cell membranes, notably improving the efficiency of viral adsorption and infection into target BC cells. To obtain stable control cell lines, infected cells were subjected to puromycin (4 μg/ml) (cat. no. HY-B1743; MedChemExpress) selection for ≥1 weeks. Stably transduced cells were maintained in medium containing the same antibiotic concentrations and used for subsequent experiments. Additionally, cell lines infected with lentivirus vectors were established. Stable cell lines were selected with puromycin (4 μg/ml) for 14 days before being used in subsequent experiments.

Western blotting analysis. Transfected cells were harvested and lysed using RIPA buffer (cat. no. R0020; Beijing Solarbio Science & Technology Co., Ltd.) supplemented with 1 mM PMSF (cat. no. HY-B0496MedChemExpress), 10 mM DTT (cat. no. HY-15917MedChemExpress), and 10 μM protein kinase inhibitor (cat. no. P1006; Beyotime Biotechnology) on ice for 30 min. Equal amounts of protein (20 μg) quantified by BCA (cat. no. PC0020; Beijing Solarbio Science & Technology Co., Ltd.) were separated by SDS-PAGE (4-20% gradient gel; cat. no. ET15420L; ACE Biotechnology) and transferred to 0.2-μm pore size PVDF membranes (cat. no. ISEQ00010; Merck Sharp & Dohme-Hoddesdon). Following the blocking of non-specific binding sites using 5% skimmed milk (cat. no. P0216; Beyotime Biotechnology) or bovine serum albumin (cat. no. NGP0028A; Beyotime Biotechnology) for 1 h at room temperature, the membranes were incubated with primary antibodies (incubation overnight at 4˚C) against DHX15 (cat. no. sc-271686; 1:1,000) and GAPDH (cat. no. sc-47724; 1:1,000; Santa Cruz Biotechnology, Inc.), and subsequently incubated with the corresponding secondary antibodies (dilution 1:1,500) for 2 h at room temperature. The secondary antibodies used were horseradish peroxidase (HRP)-conjugated goat anti-rabbit (cat. no. ZB-2301; Beijing Zhongshan Jinqiao Biotechnology Co., Ltd.) and HRP-conjugated goat anti-mouse (cat. no. ZB-2305; Beijing Zhongshan Jinqiao Biotechnology Co., Ltd.). Chemiluminescence was detected using WesternBright ECL HRP substrate (cat. no. R-03031-D2; Advansta Inc.). Bands were visualized using the C-DiGit Blot Scanner (LI-COR Biosciences), and a densitometric analysis was performed using ImageJ software (version: 1.52a) (National Institutes of Health). Three independent replicates were performed for each experimental condition.

Diagnostic and prognostic value of DHX15. The Kaplan-Meier plotter (19) database (http://kmplot.com/analysis/) was utilized to explore the association between DHX15 expression and clinical outcome (overall survival), in addition to predicting chemotherapy responses (20), in patients with BC. ROC analysis to evaluate the predictive value of DHX15 for chemotherapy pathological response was conducted via the 'ROC Plotter for Breast Cancer' module of KM Plotter. The endpoint was set as pathological response, the cohort was restricted to patients with TNBC who received any chemotherapy, and the ROC metrics were calculated using the platform's default parameters after entering the gene symbol DHX15.

Co-expression and gene enrichment analysis. The LinkedOmics database (http://www.linkedomics.org/login.php) is a web-based platform designed for the analysis of TCGA cancer-associated multi-dimensional data (21). Statistical analysis of DHX15 co-expression was performed using Pearson's correlation coefficient and visualized using a volcano plot. The 'LinkedOmics' functional module was used to analyze Gene Ontology (GO) biological processes and Kyoto Encyclopedia of Genes and Genomes (KEGG) pathway enrichment, through gene set enrichment analysis (GSEA). GSEA-based GO and KEGG enrichment analyses were conducted using the LinkedOmics database. GO and KEGG predefined gene sets were tested against the full ranked gene list correlated with DHX15. Terms with false discovery rate (FDR)<0.05 (500 permutations) were considered significantly enriched, with a minimum gene set cutoff of 2 members. GO enrichment analysis was performed, as well as PPI network analysis of DHX15-associated genes using Metascape (http://metascape.org/gp/index.html) (22).

Immune infiltration analysis. The proportion of tumor-infiltrating immune cells in TCGA-BC samples was calculated using the CIBERSORT algorithm. The correlation between the infiltration levels of 28 tumor-infiltrating immune cell types and DHX15 expression was calculated using single-sample GSEA (ssGSEA). Single-sample gene set enrichment analysis (ssGSEA) and CIBERSORT immune cell infiltration profiling were performed using the Xiantao Academic web tool (https://www.xiantao.love). Standard built-in reference signatures and default algorithm parameters were applied throughout the analysis. The CIBERSORT algorithm was invoked via the dedicated immune infiltration module of Xiantao Academic. The relative proportions of all immune cell populations within the BC samples were calculated using the platform's default parameters. For ssGSEA, the GSVA package with a KS-like non-parametric test and MSigDB immune signatures were utilized, and Wilcoxon rank-sum tests were used for subgroup comparisons after BH-FDR adjustment. In addition, the TIMER database was utilized to construct a multi-factor Cox proportional hazards model to investigate the effect of immune cell infiltration on the survival rate of patients with BC. Finally, correlations between DHX15 expression and specific invasive immune markers were estimated using the TIMER1.0 database 'Correlation' module.

Single-cell level analysis. The Human Proteome Atlas (HPA) database (https://www.proteinatlas.org) can be used to explore

the expression of DHX15 in different tumor pathology samples and across various single-cell types (23). Using the CancerSEA database (http://biocc.hrbmu.edu.cn/CancerSEA/), the biological roles of DHX15 in BC were investigated at the single-cell level (24). DHX15 was queried in the BC cohort, and Pearson correlation coefficients were calculated to evaluate its association with 14 classic malignant functional signatures using the platform's default built-in algorithm.

Immunohistochemistry (IHC) images from the HPA database. IHC staining images of DHX15 protein expression in normal and BC tissues were obtained from the HPA database (https://www.proteinatlas.org/) (23). The staining patterns and expression levels were evaluated based on the annotation provided by the HPA consortium. DHX15 protein expression levels from HPA IHC images were semi-quantitatively scored using the immunoreactive score (IRS) system, calculated as the product of staining intensity and the percentage of positively stained tumor cells. Samples were stratified into high and low expression groups based on the final IRS values. Staining intensity was scored from 0 to 3, multiplied by the percentage of positive stained cells (scored from 0-3), generating a total score ranging from 0 to 9. These H-scores were dichotomized into high and low expression groups using the median H-score of all BC samples as the cutoff value.

Wound-healing assays. All cell groups, including sh-control, sh-DHX15, MCF-7 and EX-DHX15, were seeded into 6-well plates. To eliminate the interference of cell proliferation on migration results, cells were subjected to serum starvation treatment for 12 h before scratching. Once the cells reached full confluence (~100%), a wound was created using a 100-μl sterile pipette tip, before the samples were imaged (0 h). After creating the artificial wound, the culture medium was replaced with serum-free basal DMEM without fetal bovine serum, and cells were incubated under standard cell culture conditions for the subsequent observation period. The gap closure rate was measured at 24, 48 and 96 h. In total, three independent replicates were performed for each experiment. Cells were continuously incubated at 37˚C in a humidified incubator containing 5% CO_2 during the entire wound healing observation period. Images were captured using a light microscope (80i; Nikon Corporation). Migration rate (%)=Width at time t/initial width x100.

Cell invasion and migration experiments. The migration assay was performed in a 24-well plate. DHX15-transfected MDA-MB-231 cells and MCF-7 cells were placed in the upper chamber and suspended in serum-free medium, whereas the lower chamber was filled with DMEM supplemented with 10% FBS. For the Transwell migration assays, 8-μm Transwell chambers (cat. no. 725321; Wuhan NEST Biotechnology Co., Ltd.) were used. Serum-starved cells ($1x10^4$ cells/well) were plated in the upper chambers with 100 μl FBS-free medium, and 400 μl 10% FBS medium was added to the lower chambers. The cells that migrated through the membrane were counted and images captured after 24 h. Following an overnight incubation period at 37˚C with 5% CO_2 in a humidified incubator, the cells were fixed with 100% methanol for 30 min at room temperature, and stained with 0.1% crystal violet for a duration of 20 min at room temperature. Invasion assays were performed following the same protocol as the migration assays; however, before cell seeding, the Transwell chambers were coated with Matrigel. For the Transwell invasion assays, $4x10^4$ cells in 100 μl FBS-free medium were plated in the top chamber precoated with Matrigel (cat. no. 0827045; Xiamen Mogengel Biotechnology Co., Ltd.). Matrigel was kept chilled on ice throughout all preparation steps. First, frozen Matrigel was thawed overnight at 4˚C in a refrigerator, then the Matrigel was diluted with chilled serum-free medium at a ratio of 1:2 (Matrigel:medium). Finally, the plates were placed in a humidified incubator at 37˚C for 60 min to allow the Matrigel to form a gel. Cell counting was performed using an inverted light microscope (Nikon Corporation). Each experiment was performed in triplicate.

Plate colony formation assays. A colony formation assay was performed to evaluate clonogenic survival by seeding single-cell suspensions at $1x10^3$ cells/well in 6-well plates. This experiment was conducted in the DHX15-downregulated group and the control group of MDA-MB-231 cells. After 14 days, the colonies were fixed with 100% methanol for 10 min at room temperature. Following fixation, colonies were stained with 0.1% crystal violet solution for 20 min at room temperature. Colonies were defined as clusters containing ≥50 cells or visible colonies measuring >0.1 mm in diameter. Colonies were counted manually and imaged under an inverted microscope (Nikon Corporation).

Data analysis. The statistical analysis was conducted using GraphPad Prism 9.1.0 (Dotmatics) and R software (version 4.1.2; Posit Software, PBC). Data are presented as the mean ± SD. Comparisons between two groups were performed using unpaired Student's t-tests (for independent samples), whereas multi-group comparisons were performed using one-way ANOVA, and Tukey's test was used for pairwise comparisons between groups. Survival probabilities were calculated using Kaplan-Meier analysis and differences in survival curves were assessed using the log-rank test. Gene expression correlations were quantified using Spearman's rank coefficients. All experiments were performed in triplicate. $P<0.05$ was considered to indicate a statistically significant difference.

Results

Upregulation of DHX15 mRNA expression in BC. The expression levels of DHX15 mRNA were first estimated across multiple malignant tumor types using the TIMER database. Results indicated that DHX15 mRNA expression was upregulated in BC, cholangiocarcinoma, colon adenocarcinoma, esophageal cancer, head-neck squamous cell carcinoma, liver hepatocellular carcinoma, lung adenocarcinoma, lung squamous cell carcinoma, prostate adenocarcinoma and stomach adenocarcinoma but was downregulated in kidney renal clear cell carcinoma, kidney renal papillary cell carcinoma and thyroid carcinoma (Fig. 1A). The Kaplan-Meier database results indicated that DHX15 mRNA expression levels were significantly higher in the BC group compared with those in the normal group (Fig. 1B). Receiver operating curve (ROC) analysis revealed that DHX15 exhibited an area under the

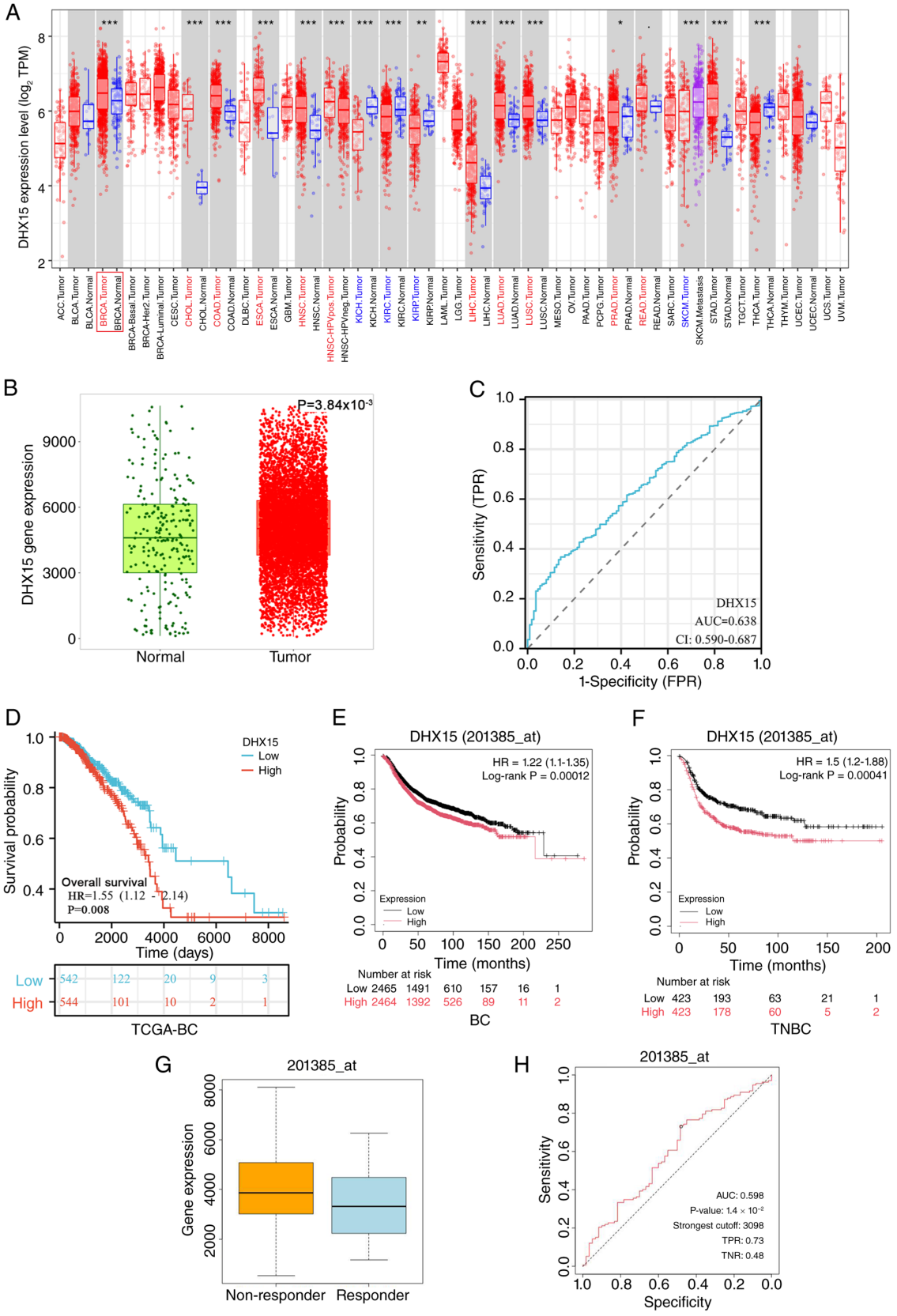

Figure 1. Upregulation of DHX15 mRNA expression in BC. (A) The expression level of DHX15 in different types of tumor tissues and normal tissues in the Tumor Immune Estimation Resource database. (B) Analysis using the Kaplan-Meier database indicating upregulated DHX15 mRNA in BC (P=0.00384). (C) ROC curve analysis of DHX15 for distinguishing patients with BC from normal (healthy cancer-free) donors (AUC=0.638; CI: 0.590-0.687). (D) Survival curves stratified by DHX15 expression levels in patients from TCGA-BRCA database (P=0.008; n=1,086). Patients were divided into high-expression and low-expression groups based on the median expression value (50%) of DHX15. The Kaplan-Meier database displays survival curves for the differentially expressed DHX15 gene in (E) patients with BC (P=0.00012; n=4,924) and (F) patients with TNBC (P=0.00041; n=846). (G) DHX15 expression levels in chemotherapy-responsive and non-responsive TNBC cases. (H) ROC curves validating the predictive value of DHX15 for chemotherapy response in patients with TNBC (AUC=0.598; P=0.014). *P<0.05, **P<0.01 and ***P<0.001. BC, breast cancer; DHX15, DEAH-box helicase 15; TPR, true positive rate; TPM, transcript per million; FPR, false positive rate; HR, hazard ratio; TNBC, triple-negative BC; ROC, receiver operating characteristic; AUC, area under the curve.

curve (AUC) value of 0.638 (P<0.05) in BC. The AUC of 0.638 was >0.5, demonstrating the preliminary diagnostic potential of DHX15 for breast cancer identification. (Fig. 1C). Patients were divided into high and low DHX15 expression groups according to the median expression level (50% percentile) for Kaplan-Meier survival analysis. Kaplan-Meier analysis demonstrated that patients with high DHX15 mRNA expression in the TCGA-BRCA dataset had a worse prognosis [hazard ratio (HR)=1.55; P<0.01; Fig. 1D]. The Kaplan-Meier database was further employed to estimate the association between DHX15 expression and patient prognosis with BC and TNBC. The present study revealed that patients with high DHX15 expression had a worse prognosis in BC (HR=1.22; P<0.001; Fig. 1E) and in TNBC (HR=1.5; P<0.001; Fig. 1F). ROC curves were next generated to validate the ability of DHX15 ability to predict chemotherapy response. Results indicated that DHX15 expression was higher in non-responders compared with that in responders amongst patients with TNBC (Fig. 1G) (P<0.05). Fig. 1H shows that the AUC was 0.598 (P<0.05), indicating a modest predictive trend of DHX15 for chemotherapy response in patients with TNBC. Consequently, these findings suggest that DHX15 may influence the prognosis of BC and could be used to develop novel biomarkers for BC.

DHX15 expression level is associated with different clinical-pathological variables and pathways among patients with BC. According to the UALCAN database, among all BC subtypes, DHX15 expression was significantly higher in the luminal, $HER2^+$ and TNBC types compared with that in normal tissues (P<0.001; Fig. 2B). Expression levels were significantly higher in tumor stages II and III compared with those in the normal group (P<0.001), with those in stage II being higher compared with those in stage III (P<0.05; Fig. 2A). Pathway analysis revealed higher expression levels of DHX15 in the p53/Rb, Hippo, WNT, Myc/Mycn, chromatin modifier and mTOR pathways compared with those in the normal group. Pathway activity changes were evaluated by Z-values, calculated as standardized differences between BC samples and normal breast tissues. Positive Z-values indicated elevated activation of all six pathways in BC compared with normal controls. (P<0.001; Fig. 2C-H). The DHX15 expression levels of N0 (no lymph node metastasis), N1 and N2 were significantly higher compared with those of normal tissues (cancer-free normal breast tissues), as indicated by the presence of lymph node metastasis (P<0.001; Fig. 2I). The prognostic relevance of DHX15 in patients with BC was also explored. The results suggested that amongst patients in stage T2, T3 and T4, as well as those in stages II and III, shorter survival times were associated with higher levels of DHX15 expression (both P<0.01; Fig. 2L and N). Additionally, Fig. 2J, K and M displayed the IHC staining results of DHX15 in the high-expression group and low-expression group (P<0.001). HPA IHC images and semi-quantitative scoring validated the upregulation of DHX15 at the protein level, consistent with the mRNA-level bioinformatics results. Representative high/low staining pictures directly visualized DHX15 expression heterogeneity in clinical BC tissues, and the statistical comparison further supported that DHX15 upregulation is a common feature in BC, preliminarily supporting its potential value as a pathological biomarker.

DHX15 co-expression gene and pathway enrichment in BC. Genes co-expressed with DHX15 were screened and their expression patterns were visualized via a volcano plot in BC, thereby advancing understanding of the DHX15 mechanism of action (Fig. 3A). The 50 most significant genes positively or negatively correlated with DHX15 are also displayed (Fig. 3B and C). Subsequently, pathway enrichment analysis was employed to further investigate the role of co-expressed genes with DHX15 in BRCA. GO enrichment analysis revealed that genes co-expressed with DHX15 were primarily enriched in 'microtubule cytoskeleton organization involved in mitosis', 'double-strand break repair' and 'protein polyubiquitination' (Fig. 3D). KEGG enrichment analysis indicated that these genes were primarily enriched in the 'ubiquitin-mediated proteolysis' pathway (Fig. 3E).

Metascape analysis indicated that the top 50 positive and top 50 negative genes with DHX15 were mainly clustered in the 'signal recognition particle (SRP)-dependent co-translational protein targeting to the rough endoplasmic reticulum', 'DNA repair' and 'chemical carcinogenesis-reactive oxygen species' (Fig. 4A). The PPI network of the first 100 genes co-expressed with DHX15 were primarily enriched in RNA metabolism, 'SRP-dependent co-translational protein targeting to the membrane' and the 'response of EIF2AK4 (GCN2) to amino acid deficiency' (Fig. 4B and D). Furthermore, MCODE profiling indicated that DHX15 and its neighboring genes may influence 'SRP-dependent co-translational protein targeting to membrane', 'ribosome, cytoplasmic' and 'cytoplasmic ribosomal proteins' (Fig. 4C and E). In summary, these findings indicate that genes co-expressed with DHX15 are primarily involved in translational protein localization and DNA repair processes within BC. Based on these findings, it is hypothesized that DHX15 participates in regulating cellular transcription processes.

Analysis of DHX15 at the single cell level in BC. The HPA database revealed the three most prominent single cells exhibiting DHX15 expression in BC are breast glandular cells, T cells and macrophages. While DHX15 expression is moderate in endothelial cells and adipocytes, these cell types account for a relatively small proportion of the total. DHX15 is predominantly expressed in breast glandular cells, with a mean of 73.2 standardized transcripts per million protein-coding genes across all cell lines (Fig. 5A). Furthermore, the differential expression levels of DHX15 facilitated the clustering of cells into distinct populations. DHX15 is mainly expressed in the c-21 cell cluster (breast glandular cells). Fig. 5B presents the varying expressions levels of DHX15 and established cell type markers across the distinct BC cell clusters. In breast glandular cells, clusters demonstrated higher expression of ESR1 and forkhead box A1 (FOXA1), which is positively correlated with DHX15 (Fig. 5B). Subsequently, the CancerSEA database was utilized to analyze the association between DHX15 expression levels and individual BC single-cell biological functions. The results indicated that DHX15 expression was positively associated with DNA damage, the cell cycle, DNA repair, stemness and invasion (Fig. 5C). Xenograft models from the database were used to further validate these biological functions. Results indicated that DHX15 expression was positively associated with the cell cycle and DNA damage, but negatively

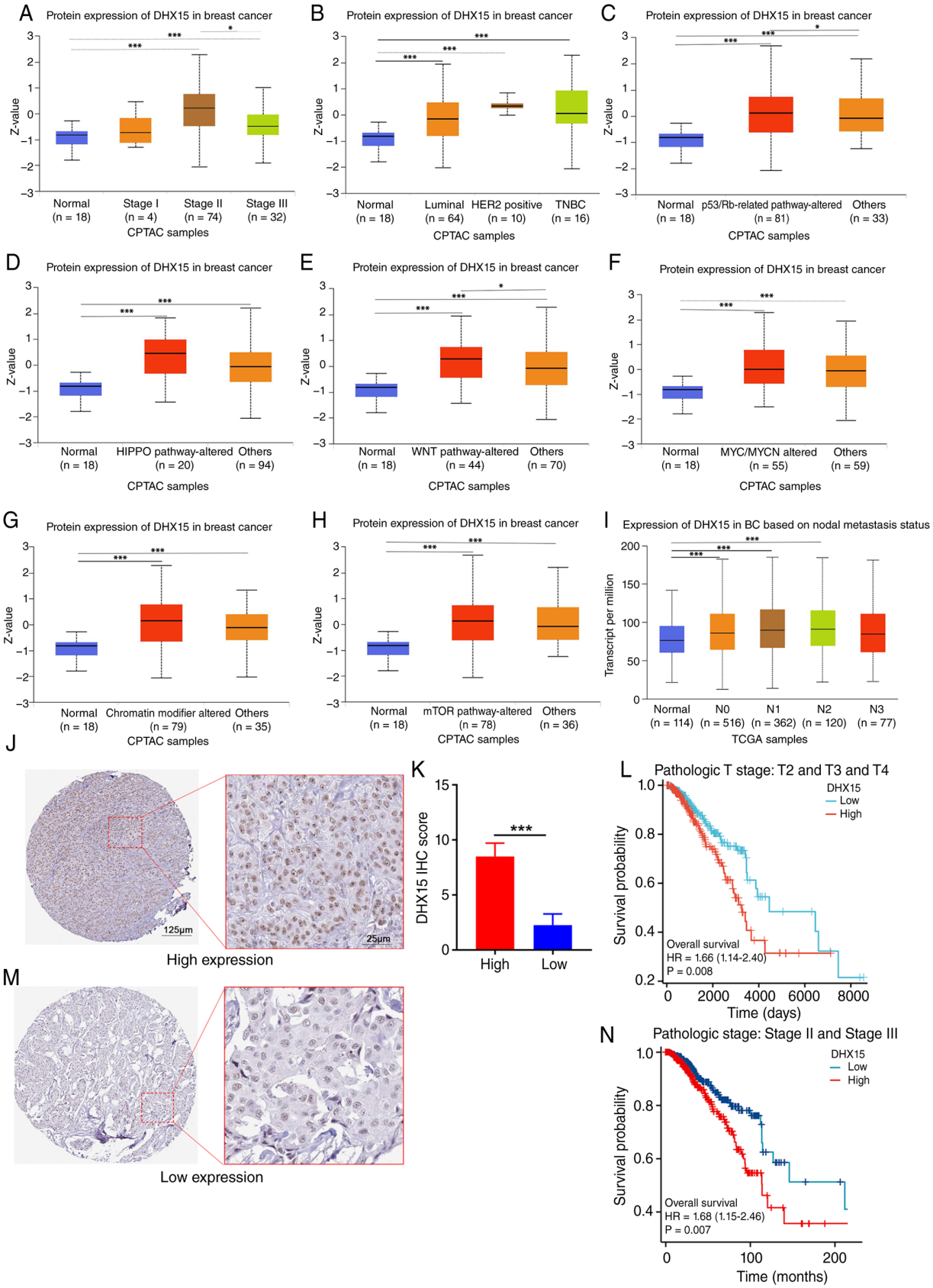

Figure 2. DHX15 expression levels are associated with different clinicopathological variables and pathways among patients with BC. In the University of Alabama at Birmingham Cancer database, an association was observed between DHX15 protein expression and (A) stage, (B) subtypes, (C) p53/Rb, (D) Hippo, (E) WNT, (F) Myc/Mycn, (G) chromatin modifier and (H) mTOR pathways. (I) Association between DHX15 mRNA expression and lymph node metastasis status. (L) Patients with T2, T3 and T4 stages (P=0.008) and (N) patients with stage II and III disease (P=0.007) Representative IHC images of DHX15 protein expression in (J) high and (M) low expression BC tissues, with (K) unpaired Student's t-tests (n=12; P<0.001). Images (J) and (M) were obtained from the Human Protein Atlas database (https://www.proteinatlas.org/). (J and M) Association of DHX15 expression with the prognosis of patients with BC at different clinical stages. *P<0.05 and ***P<0.001. BC, breast cancer; CPTAC, clinical proteomic tumor analysis consortium; DHX15, DEAH-box helicase 15; TNBC, triple-negative BC; TCGA, The Cancer Genome Atlas; IHC, immunohistochemistry.

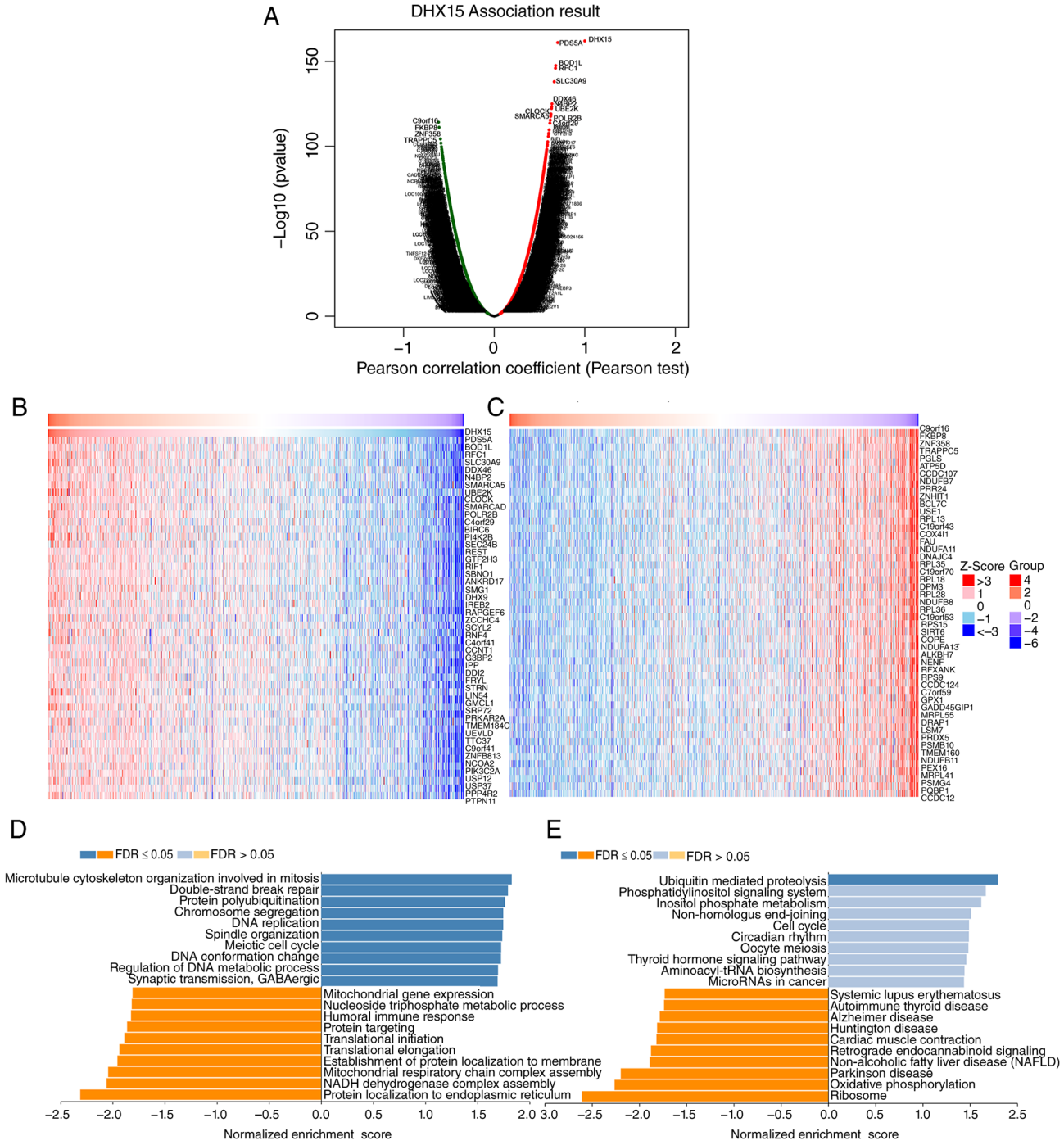

Figure 3. Results of DHX15 co-expression analysis. (A) Volcano plot; red dots indicate genes positively correlated with DHX15, while green dots indicate genes negatively correlated. (B) Heatmap showing the top 50 genes positively correlated with DHX15. (C) Heatmap demonstrating the top 50 genes negatively correlated with DHX15. (D) Gene Ontology enrichment analysis. (E) Kyoto Encyclopedia of Genes and Genomes enrichment analysis. DHX15, DEAH-box helicase 15; FDR, false discovery rate.

associated with hypoxia (Fig. 5D). These findings further reveal the potential biological functions of DHX15 in BRCA, particularly at the single-cell level.

Correlation between DHX15 and immune infiltration in BC through bioinformatics analysis. The present study investigated the correlation between DHX15 expression and immune cell infiltration in patients with BC. ssGSEA analysis and CIBERSORT analysis were conducted to examine this correlation. The ssGSEA results indicated a significant positive association between DHX15 expression and T helper cells (R=0.413; P<0.001), and central memory T cell (Tcm) (R=0.34; P<0.001), and DHX15 expression had a weak positive association with T helper 2 (Th2) cell infiltration (R=0.263; P<0.001). A negative significant correlations were found with plasmacytoid dendritic cells(pDC) (R=-0.408; P<0.001), and a weak negative association with cytotoxic cells (R=-0.266; P<0.001), DCs (R=-0.234; P<0.001), NK cells (R=-0.206; P<0.001), $CD8^+$ T cell infiltration (R=-0.196; P<0.001) and B cells (R=-0.122; P<0.001; Fig. 6A). The CIBERSORT results indicated a weak

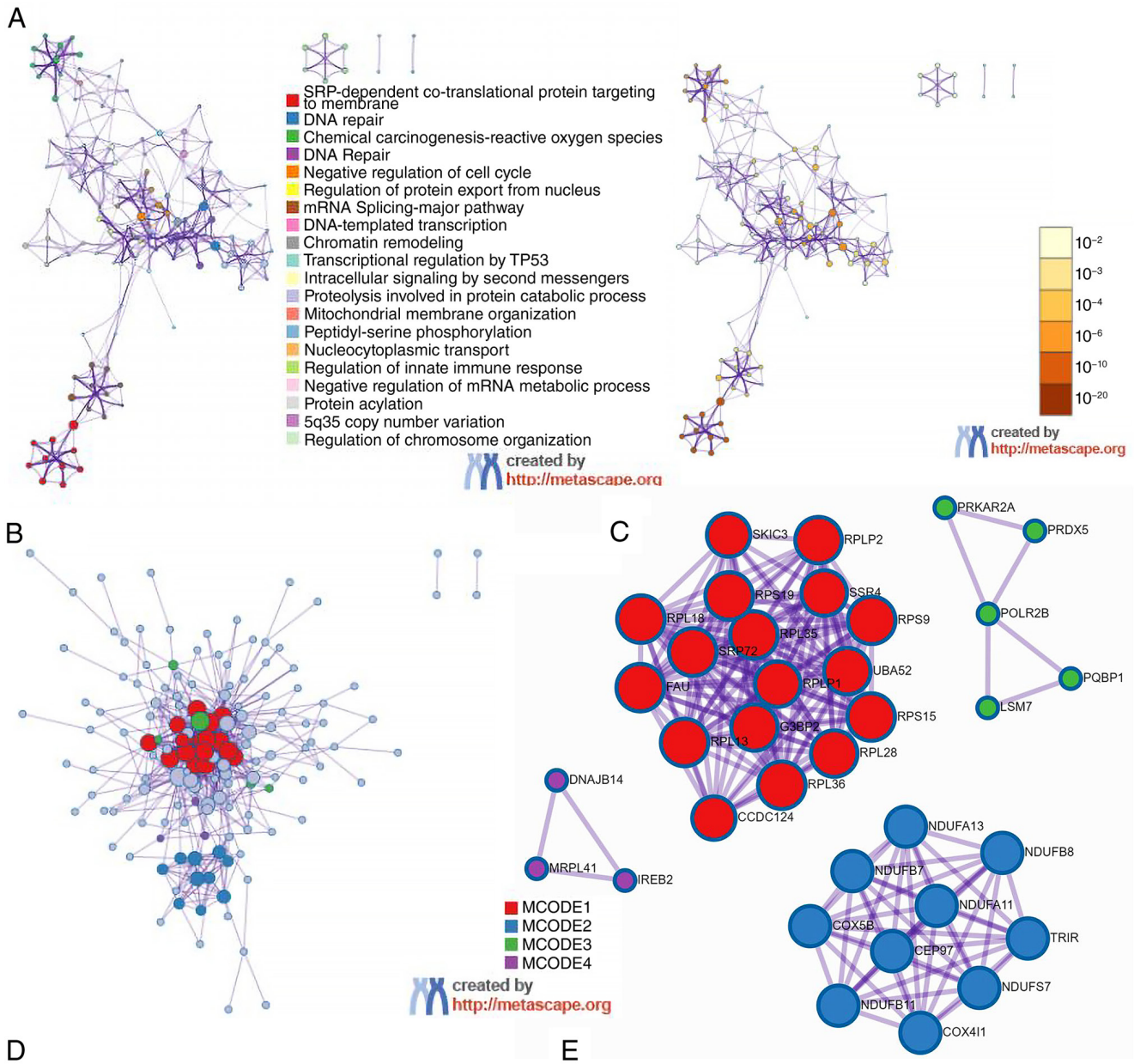

D

GO	Description	log_{10}(P-value)
R-HSA-8953854	Metabolism of RNA	-15.5
R-HSA-1799339	SRP-dependent cotranslational protein targeting to membrane	-15.4
R-HSA-9633012	Response of EIF2AK4 (GCN2) to amino acid deficiency	-14.5

E

Color	MCODE	GO	Description	log_{10}(P-value)
	MCODE_1	R-HSA-1799339	SRP-dependent cotranslational protein targeting to membrane	-31.5
	MCODE_1	CORUM:306	Ribosome, cytoplasmic	-27.5
	MCODE_1	WP477	Cytoplasmic ribosomal proteins	-27.0
	MCODE_2	GO:0006119	oxidative phosphorylation	-17.8
	MCODE_2	hsa00190	Oxidative phosphorylation	-17.2
	MCODE_2	WP4396	Nonalcoholic fatty liver disease	-16.8
	MCODE_3	R-HSA-72163	mRNA Splicing - Major Pathway	-5.5
	MCODE_3	R-HSA-72172	mRNA Splicing	-5.5
	MCODE_3	R-HSA-72203	Processing of Capped Intron-Containing Pre-mRNA	-5.1

Figure 4. PPI analysis of DHX15 and its co-expressed genes in breast cancer. (A) Clustered pathway analysis of the co-expressed genes of DHX15. On the left is the annotation of the cluster pathway enriched for co-expressed genes; on the right, the expression level of each cluster is represented by the intensity of the color, with darker shades indicating a stronger correlation. (B) DHX15 and its associated genes within the constructed PPI network. (C) DHX15 and its co-expressed genes associated with MCODE modules. (D) Annotations for PPI network. (E) Annotations for MCODE modules. DHX15, DEAH-box helicase 15; SRP, signal recognition particle; EIF2AK4, eukaryotic translation initiation factor 2 α kinase 4; GCN2, general control nonderepressible 2; PPI, protein-protein interaction.

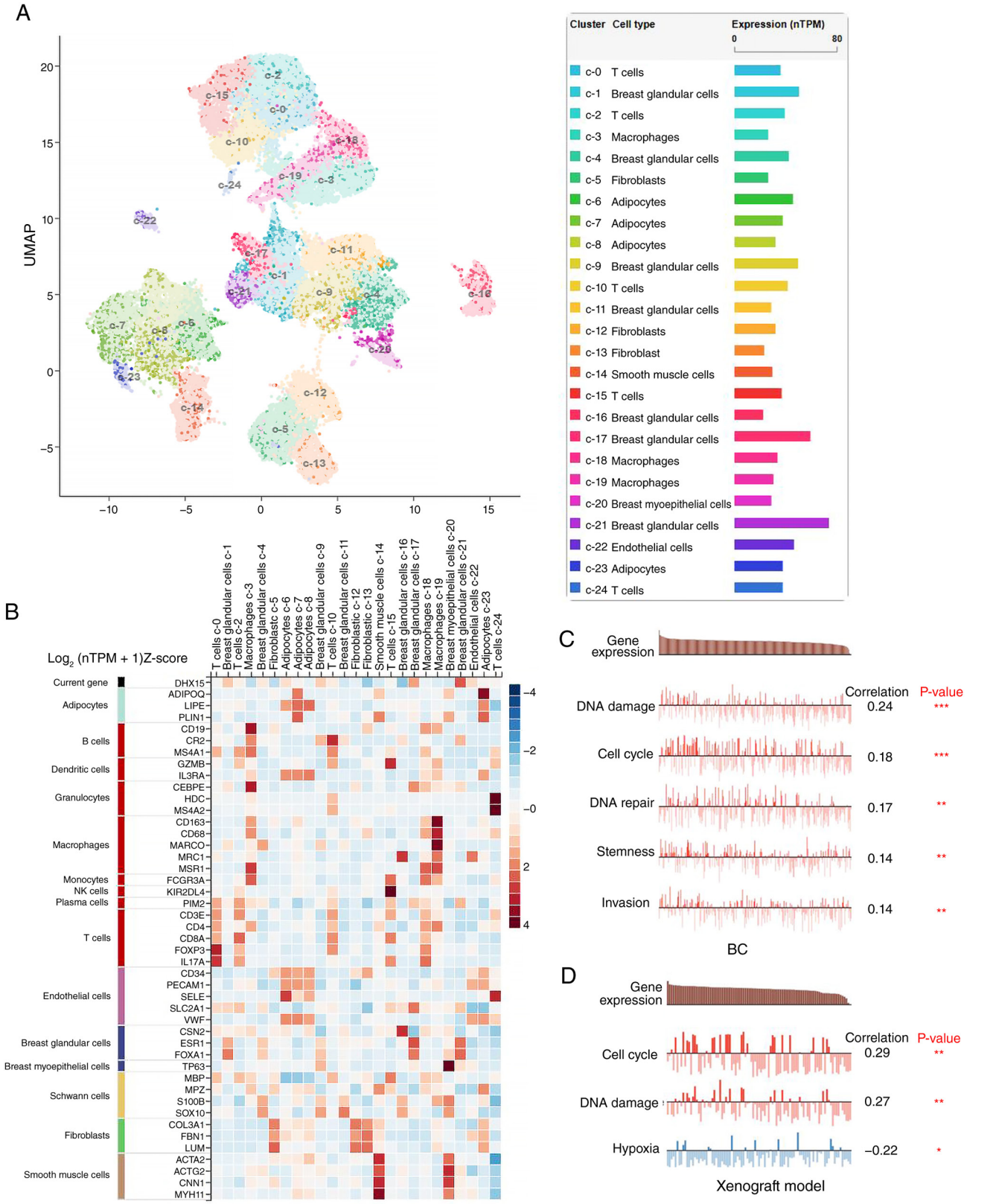

Figure 5. Analysis of DHX15 at the single-cell level in BC. (A) Expression profile of DHX15 across BC cell clusters. (B) Expression level of DHX15 and cell type markers in various cell clusters of BC. Association between DHX15 and single-cell biological functions in (C) BC and (D) xenograft models based on the CancerSEA database. *P<0.05, **P<0.01 and ***P<0.001. BC, breast cancer; DHX15, DEAH-box helicase 15; UMAP, Uniform Manifold Approximation and Projection; nTPM, normalized transcripts per million.

positive association between DHX15 expression and resting CD4^{+} memory T cells (R=0.217; P<0.001) and M2 macrophages (R=0.152; P<0.001), with negative weak associations with regulatory T cells [(Tregs); R=-0.295; P<0.001], CD8^{+} T cells (R=-0.163; P<0.001), activated NK cells (R=-0.134; P<0.001) and memory B cells (R=-0.119; P<0.001; Fig. 6B).

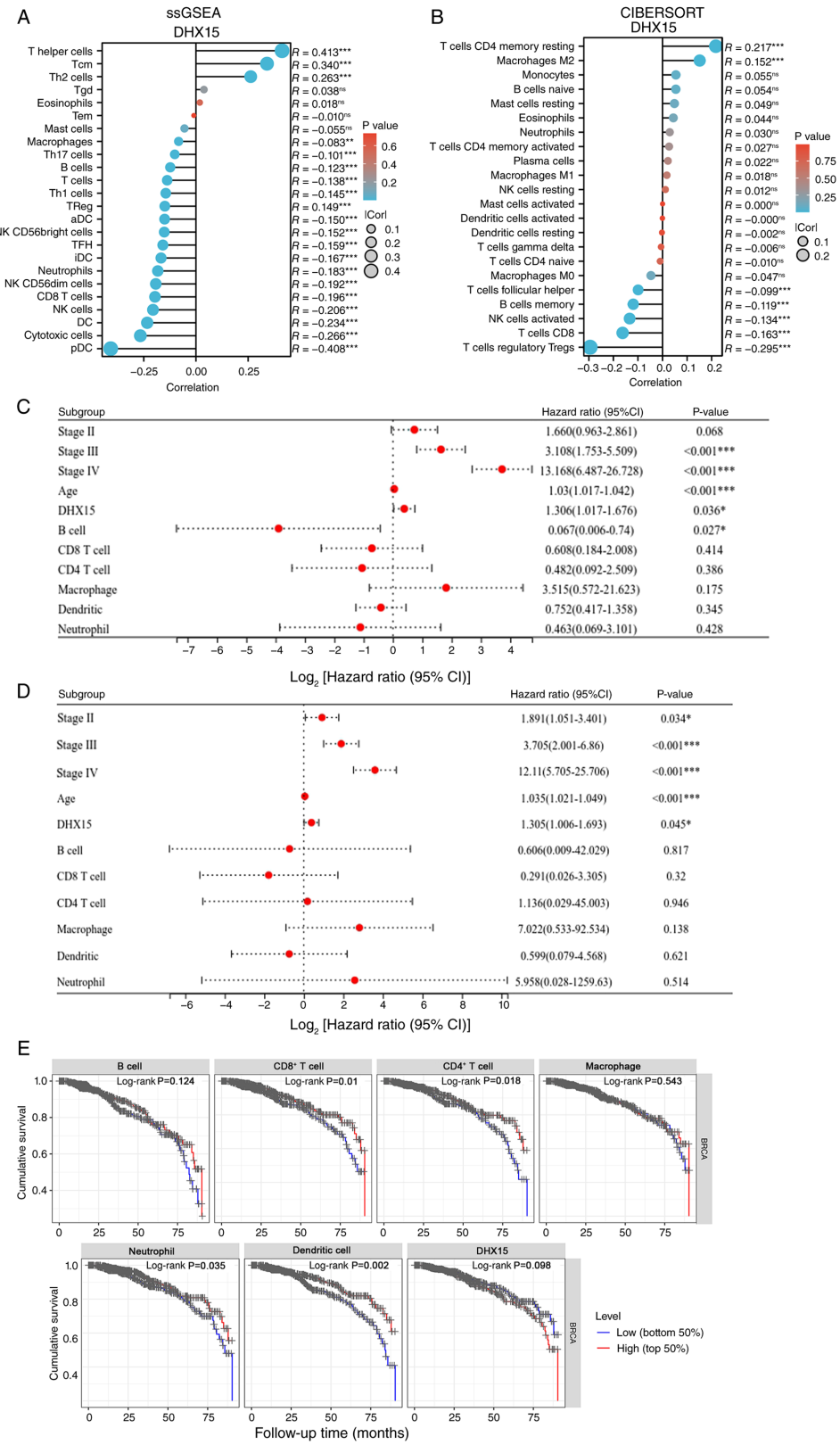

Figure 6. Correlation between DHX15 and immune infiltration in BC was analyzed using bioinformatics analysis. (A) ssGSEA analysis demonstrates a comparison of infiltration and DHX15 expression across distinct immune cell types (cut-off value is the median). (B) CIBERSORT analysis shows immune cell types infiltration and DHX15 expression (cut-off value is the median). (C) Univariate Cox screening of all candidate prognostic factors. (D) Multivariable Cox proportional hazards models were used to evaluate the impact of DHX15 expression on survival, adjusted for the infiltration levels of multiple immune cells. DHX15 expression was stratified by the median cutoff value, with low expression as the reference. Age and immune cell infiltration levels were analyzed as continuous covariates. Stages II, III, and IV were each compared separately to Stage I. (E) Kaplan-Meier plots illustrating the association between DHX15 expression and immune infiltration status in BC. Each survival curve corresponds to a combined subgroup defined by both DHX15 expression level and immune cell infiltration status. *P<0.05, **P<0.01 and ***P<0.001. BC, breast cancer; DHX15, DEAH-box helicase 15; ssGSEA, single-sample gene set enrichment analysis; NK, natural killer; Treg, regulatory T cell; Tem, Tcm, Tgd, TFH, aDC, iDC, pDC; ns, not significant; Cor, correlation. Tem, effector memory T cell; Tcm, Ccentral memory T cell; Tgd, γδ T cell; TFH, follicular helper T cell; aDC, activated dendritic cell; iDC, immature dendritic cell; pDC, plasmacytoid dendritic cell.

Table I. Correlation analysis between DEAH-box helicase 15 and immune cell markers in the Tumor Immune Estimation Resource database.

		Breast cancer			
		Unadjusted		Purity-adjusted	
Description	Gene markers	Cor	P-value	partial.cor	partial.P-value
$CD8^+$ T cell	CD8A	-0.006	$8.53x10^{-1}$	0.064	$4.44x10^{-2a}$
	CD8B	-0.110	$2.50x10^{-4b}$	-0.055	$8.55x10^{-2}$
T cell (general)	CD3D	-0.129	$1.84x10^{-5b}$	-0.077	$1.52x10^{-2a}$
	CD3E	-0.083	$5.99x10^{-3a}$	-0.020	0.53
	CD2	-0.037	$1.50x10^{-1}$	0.027	0.40
B cell	CD19	-0.094	$1.84x10^{-3a}$	-0.056	$7.60x10^{-2a}$
	CD79A	-0.092	$2.21x10^{-3a}$	-0.046	0.15
Monocyte	CD86	0.115	$1.40x10^{-4c}$	0.176	$2.32x10^{-8b}$
	CD115 (CSF1R)	0.076	$1.19x10^{-2}$	0.133	$2.47x10^{-5b}$
TAM	CCL2	-0.018	$5.59x10^{-1}$	0.040	0.21
	CD68	0.081	$7.44x10^{-3a}$	0.129	$4.30x10^{-5b}$
	IL10	0.160	$1.03x10^{-7b}$	0.216	$5.75x10^{-12b}$
M1 macrophage	INOS (NOS2)	0.061	$4.29x10^{-2a}$	0.073	$2.10x10^{-2a}$
	IRF5	0.031	0.3	0.048	0.13
	COX2 (PTGS2)	0.085	$4.95x10^{-3a}$	0.146	$3.99x10^{-6b}$
M2 macrophage	CD163	0.190	$1.98x10^{-10b}$	0.243	$8.58x10^{-15b}$
	VSIG4	0.112	$1.99x10^{-4c}$	0.159	$4.89x10^{-7b}$
	MS4A4A	0.121	$5.82x10^{-5b}$	0.193	$8.75x10^{-10b}$
Neutrophils	CD66b (CEACAM8)	0.016	$6.05x10^{-1}$	0.011	0.72
	CD11b (ITGAM)	0.160	$1.02x10^{-7b}$	0.199	$2.42x10^{-10b}$
	CCR7	-0.020	$5.08x10^{-1}$	0.048	0.13
Natural killer cell	KIR2DL1	-0.016	$5.87x10^{-1}$	0.003	0.91
	KIR2DL3	-0.006	$8.45x10^{-1}$	0.017	0.60
	KIR2DL4	-0.055	$6.66x10^{-2}$	-0.015	0.64
	KIR3DL1	-0.008	$7.89x10^{-1}$	0.022	0.50
	KIR3DL2	-0.044	$1.42x10^{-1}$	-0.012	0.71
	KIR3DL3	-0.012	$7.02x10^{-1}$	-0.004	0.90
	KIR2DS4	-0.042	$1.63x10^{-1}$	-0.009	0.78
Dendritic cell	HLA-DPB1	-0.138	$4.43x10^{-6b}$	-0.098	$1.90x10^{-3a}$
	HLA-DQB1	-0.102	$6.66x10^{-4b}$	-0.062	$5.25x10^{-2}$
	HLA-DRA	0.037	$2.16x10^{-1}$	0.101	$1.44x10^{-3a}$
	HLA-DPA1	0.032	$2.93x10^{-1}$	0.099	$1.84x10^{-3a}$
	BCDA-1 (CD1C)	-0.022	$4.61x10^{-1a}$	0.045	0.15
	BCDA-4 (NRP1)	0.244	$2.29x10^{-16b}$	0.300	$4.30x10^{-22b}$
	CD11c (ITGAX)	0.068	$2.42x10^{-2a}$	0.135	$1.91x10^{-5b}$
Th1	T-bet (TBX21)	-0.078	$1.00x10^{-2a}$	-0.023	0.46
	STAT4	0.056	$6.28x10^{-2}$	0.134	$2.23x10^{-5b}$
	STAT1	0.285	$6.24x10^{-22b}$	0.305	$8.23x10^{-23b}$
	IFN-γ (IFNG)	-0.039	$1.91x10^{-1}$	0.002	0.94
	TNF-α (TNF)	0.053	$8.02x10^{-2}$	0.076	$1.62x10^{-2a}$
Th2	GATA3	0.266	$3.18x10^{-19b}$	0.240	$1.64x10^{-14b}$
	STAT6	0.236	$2.39x10^{-15b}$	0.249	$1.83x10^{-15b}$
	STAT5A	0.057	$5.84x10^{-2}$	0.088	$5.32x10^{-3a}$
	IL13	-0.021	$4.87x10^{-1}$	0.010	0.74
Tfh	BCL6	0. 200	$2.01x10^{-11b}$	0.228	$3.74x10^{-13b}$
	IL21	0.049	$1.05x10^{-1}$	0.078	$1.35x10^{-2a}$
Th17	STAT3	0.451	$4.19x10^{-56b}$	0.454	$1.39x10^{-51b}$
	IL17A	-0.029	$3.33x10^{-1}$	-0.021	0.50

Table I. Continued.

Description	Gene markers	Breast cancer			
		Unadjusted		Purity-adjusted	
		Cor	P-value	partial.cor	partial.P-value
Treg	FOXP3	0.033	$2.72x10^{-1}$	0.098	$2.05x10^{-3a}$
	CCR8	0.236	$2.05x10^{-15}$	0.288	$2.07x10^{-20}$
	STAT5B	0.328	$5.62x10^{-29}$	0.341	$1.77x10^{-28}$
	TGFβ (TGFB1)	-0.034	$2.55x10^{-1}$	0.007	0.816
T cell exhaustion	PD-1 (PDCD1)	-0.134	$7.99x10^{-6}$	-0.091	$4.02x10^{-3}$
	CTLA4	-0.033	$2.75x10^{-1}$	0.021	0.51
	LAG3	-0.160	$1.03x10^{-7}$	-0.131	$3.23x10^{-5}$
	TIM-3 (HAVCR2)	0.140	$3.39x10^{-6}$	0.193	$7.78x10^{-10}$
	GZMB	-0.110	$2.64x10^{-4}$	-0.074	$1.96x10^{-2}$

[a]P<0.05, [b]P<0.001 and [c]P<0.01. Cor, R value of Spearman's correlation; None, correlation without adjustment. Purity, correlation adjusted by purity. Th, T helper cell; Tfh, T follicular helper cell; TAM, tumor-associated macrophages; Treg, regulatory T cell.

Consistent positive correlations were observed in two independent algorithms: ssGSEA revealed a positive association between DHX15 and TCM signatures, while CIBERSORT further confirmed this trend in resting CD4 memory T cells. Univariate Cox regression analysis was initially performed for all candidate variables. DHX15 expression showed significant prognostic value (P<0.05); Stage III, Stage IV and age also showed statistical significance. Several immune cell variables exhibited P>0.05 in univariate analysis, but they were still incorporated into the multivariate model due to their well-established clinical prognostic relevance in breast cancer (Fig. 6C). In addition, the Cox proportional hazard model was applied for DHX15 expression, six tumor-infiltrating immune cell types, stage II-IV and age in BC. As presented in Fig. 6D, stage II (P<0.05), stage III (P<0.001), stage IV (P<0.001), age (P<0.001) and DHX15 (P<0.05) were revealed to be significantly associated with overall survival in patients with BC. Furthermore, the TIMER1.0 database was utilized to conduct further survival analysis of DHX15 in the context of immune cell infiltration. The results indicated that based on the DHX15 high- and low-expression groups, the infiltration of $CD8^+$ T cells (P<0.05), $CD4^+$ T cells (P<0.05) neutrophil cells (P<0.05) and dendritic cells (P<0.01) was significantly correlated with the prognosis of BC. (Fig. 6E).

Spearman's correlation analysis was employed to evaluate the association between DHX15 expression and immune cell markers in TCGA data, adjusting for tumor purity. As presented in Table I, a marked positive correlation was observed between DHX15 expression and monocyte (CD86 and colony-stimulating factor 1 receptor), tumor associated macrophage (CD68 and IL10), M1 macrophage (nitric oxide synthase 2 and cyclooxygenase-2), M2 macrophage (CD163, V-set and immunoglobulin domain-containing 4 and membrane-spanning 4-domains A4A), Th1 (STAT4, STAT1 and TNF), Th2 (GATA-binding protein 3, STAT6 and STAT5A), Th17 (STAT3), T follicular helper cell (BCL6 and IL21) and Treg (FOXP3, C-C motif chemokine receptor 8 and STAT5B) markers. In addition, DHX15 was negatively correlated with $CD8^+$ T cell (CD8B), B cell (CD19A, CD79A) and T cell exhaustion [programmed cell death 1 (PDCD1), lymphocyte-activation gene 3 (LAG3) and granzyme B (GZMB)] markers.

DHX15 enhances proliferation, migration and invasion in BC cells. The aforementioned preliminary bioinformatics analysis revealed the biological function of DHX15 in BC. Given that DHX15 is highly expressed in both BC tissues and cells, and bioinformatics analysis indicates that patients with high expression associate with worse outcomes, it was hypothesized that DHX15 serves a key role in BC progression. The endogenous RNA and protein expression levels of DHX15 in BC cells was analyzed using data from the HPA database (Fig. S1). The results suggested that DHX15 exhibited notably higher endogenous expression at both the mRNA and protein levels in MDA-MB-231 cells compared with MCF-7 cells. To validate the present hypothesis, stably transfected cell lines were constructed by downregulating DHX15 in MDA-MB-231 cells and upregulating DHX15 in MCF-7 cells. Western blotting revealed that DHX15 expression levels were reduced in sh-DHX15-transfected MDA-MB-231 cells (Fig. 7A) and were increased in EX-DHX15- transfected MCF-7 cells (Fig. 8A). Wound healing experiments indicated that knockdown of the DHX15 gene resulted in delayed healing (P<0.001; Fig. 7B and C). By contrast, overexpression of the DHX15 gene resulted in accelerated healing (P<0.01; Fig. 8B and C). Transwell assays demonstrated that knocking down DHX15 expression resulted in reduced migration and invasion capabilities of MDA-MB-231 cells (P<0.001; Fig. 7D and E), but overexpression of DHX15 resulted in increased migration and invasion capabilities of MCF-7 cells (P<0.001; Fig. 8D and E). Furthermore, DHX15 knockdown led to a decrease in the number of colonies formed (P<0.001; Fig. 7F and G). Colony formation assay was performed only in DHX15-knockdown MDA-MB-231 cells, as MCF-7 cells display slow proliferation

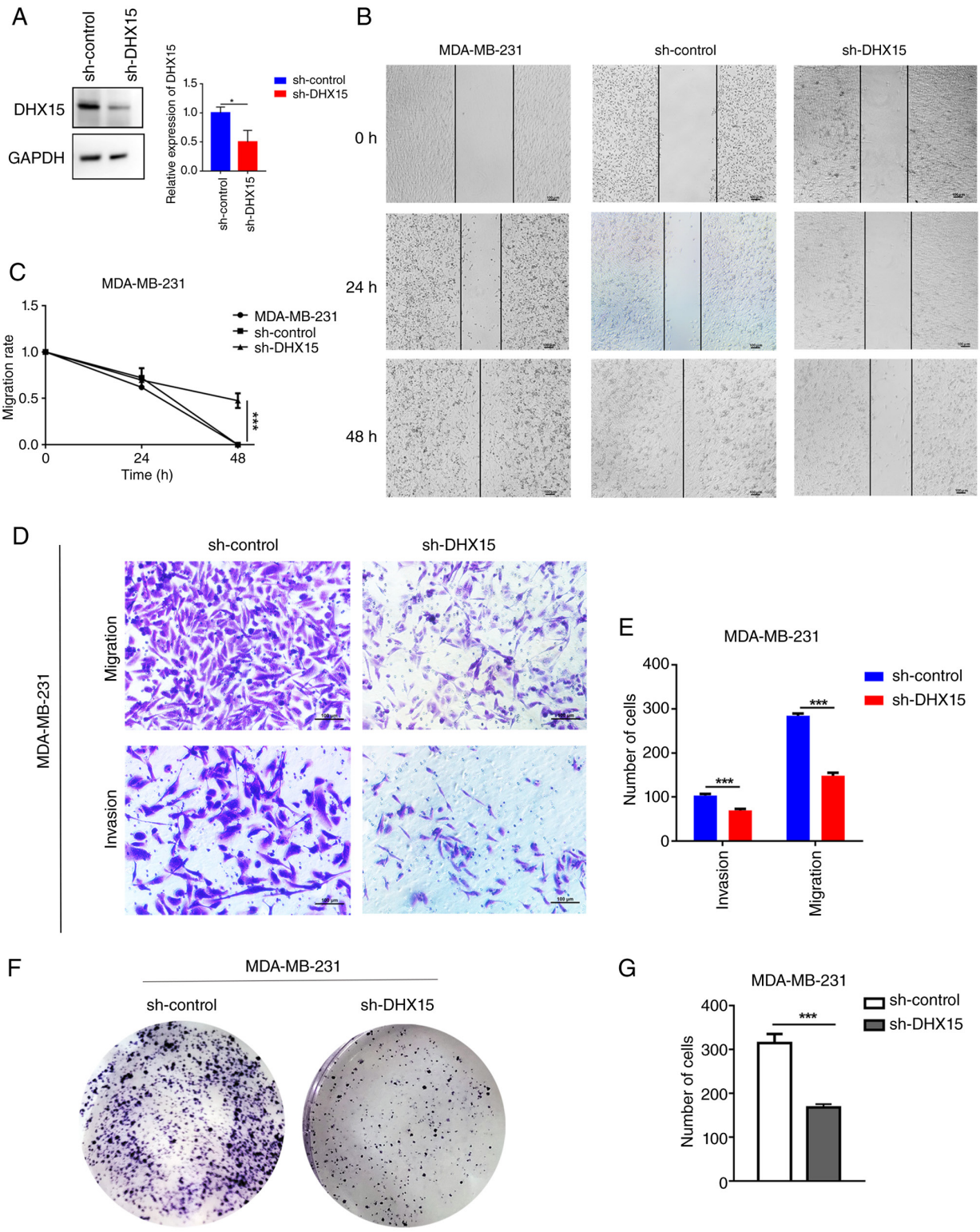

Figure 7. DHX15 promotes proliferation, migration and invasion in MDA-MB-231 cells. (A) Western blot analysis of sh-DHX15 and sh-control cells (unpaired Student's t-tests). (B) Wound-healing assays conducted on sh-DHX15-transfected MDA-MB-231 cells and (C) semi-quantification of wound-healing assay results (one-way ANOVA and Tukey's test). (D) Migration and invasion assays conducted for sh-DHX15-transfected MDA-MB-231 cells and (E) semi-quantification of migration and invasion assay results (unpaired Student's t-tests). (F) Colony formation assay performed on sh-DHX15-transfected MDA-MB-231 cells and (G) semi-quantification of colony formation assay (unpaired Student's t-tests). Scale bars, 100 μm. Data are presented as mean ± SD. Each experiment was performed in three individual replicates. *P<0.05 and ***P<0.001. sh, short hairpin; DHX15, DEAH-box helicase 15.

and poor colony-forming capacity for this assay under conventional culture conditions. Therefore, the knockdown of DHX15 may inhibit the proliferation, migration and invasion of MDA-MB-231 cells.

Discussion

BC remains a key issue in the realm of global health challenges. The complex pathogenesis and varied clinical manifestations

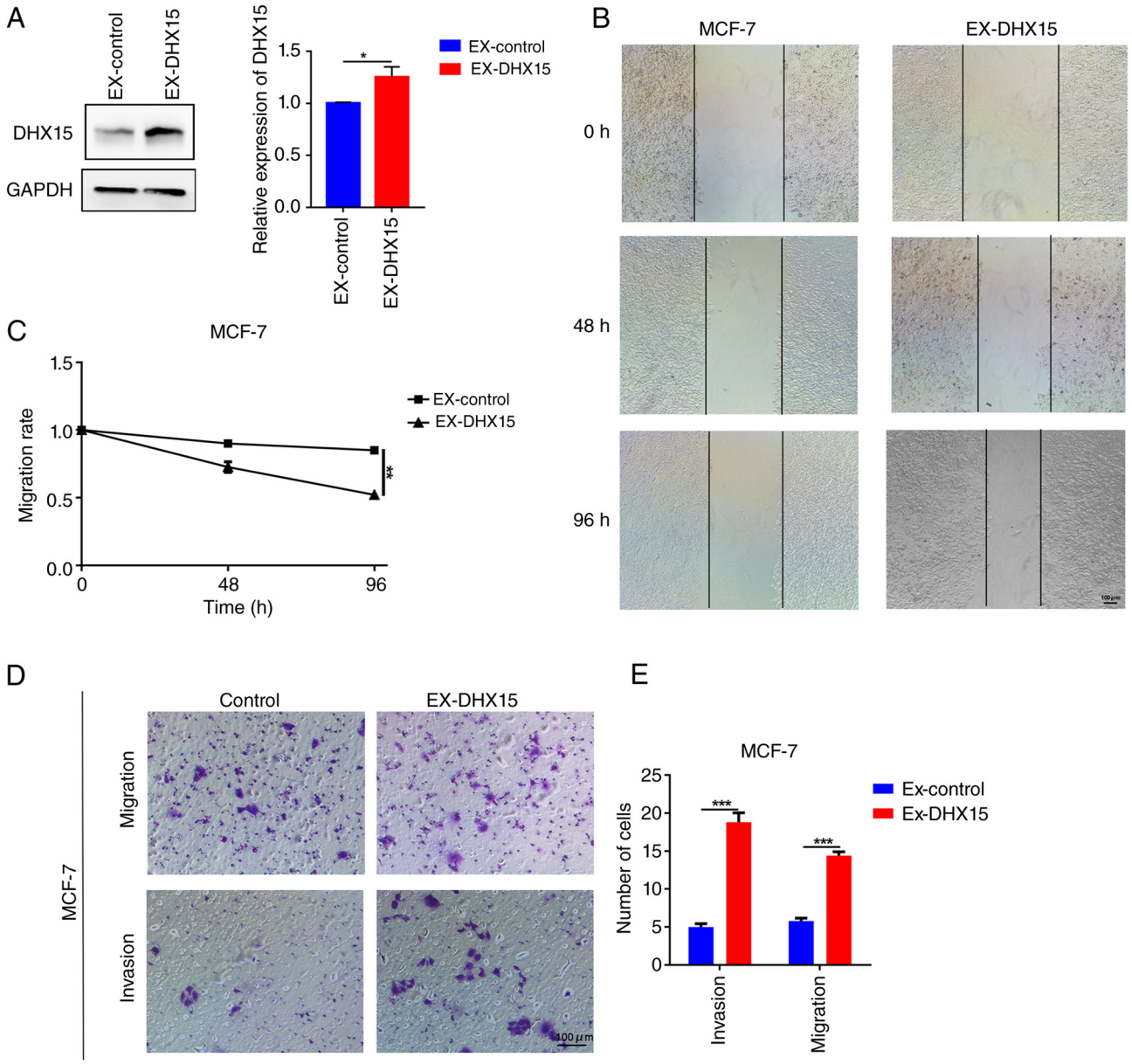

Figure 8. DHX15 promotes proliferation, migration and invasion of MCF-7 cells. (A) Western blotting analysis of MCF-7-EX-DHX15 and EX-control cells (unpaired Student's t-tests). (B) Wound-healing assays conducted on DHX15-transfected MCF-7 cells and (C) semi-quantification of wound-healing assay results (unpaired Student's t-tests). (D) Migration and invasion assays conducted for DHX15-transfected MCF-7 cells and (E) semi-quantification of migration and invasion assay results (unpaired Student's t-tests). Data are presented as means ± SD. Each experiment was performed in 3 individual replicates. *P<0.05, **P<0.01 and ***P<0.001. EX, exogenous overexpressed; DHX15, DEAH-box helicase 15.

of BC pose notable obstacles to effective treatment and prevention (1). Therefore, it is key to characterize novel biomarkers for BC to detect and treat the disease. As a member of the DEAD-box RNA-unwinding subfamily, DHX15 is a key regulator of mRNA maturation and ribosome assembly (25). Previous studies through experiments have demonstrated that DXH15 is notably overexpressed in hepatocellular carcinoma and serves a key role in controlling hepatocellular carcinoma tumor growth and expansion (12,13,26,27). This indicates that DHX15 serves a key role in the invasive behavior of hepatocellular carcinoma and may serve as a biomarker for migratory potential. Furthermore, high expression of DHX15 can promote the progression of prostate cancer by stimulating siah 2-mediated ubiquitination of the androgen receptor (26), whereas upregulated DHX15 in BC is associated with worse prognosis in patients (28). Nonetheless, the biological function and molecular regulatory mechanisms in BC development remain incompletely elucidated. Building on this foundation, the present study utilized TCGA, the Kaplan-Meier database, Metascape, wound-healing assays, Transwell assays and colony formation experiments to investigate DHX15 as a potential therapeutic target and biomarker for BC. The present study focused on gene expression levels, predictive abilities, immune cell infiltration, protein interaction network construction, single-cell functional analysis, pathway analysis and molecular mechanisms.

From the analysis of GO, KEGG and PPI networks, the present study demonstrated that DHX15 and its co-expressed genes were enriched in certain pathways, such as 'microtubule cytoskeleton organization involved in mitosis', SRP-dependent

cotranslational protein targeting to membrane' and 'DNA repair'. The CancerSEA database indicated that the biological function of DHX15 in BC single-cell data was primarily associated with DNA damage, cell cycle, DNA repair, stemness and invasion. The present results indicated that DHX15 may enhance tumor malignancy by promoting transcriptional regulation and cell cycle control in BC cells. Consistent research indicates that DHX15 enhances androgen receptor transcriptional activity and contributes to prostate cancer progression through Siah2 (26).

The tumor immune microenvironment (TIME) is considered the environment surrounding the tumor. The composition of the TIME is chiefly constituted by immune cells and cytokines, which are mainly produced by tumor cells (29). The degree of immune cell infiltration in tumor tissue is associated with the malignancy of the tumor (30). Regulatory cells of the TIME, including Th2, tumor-associated macrophage (TAMs), Tregs and myeloid-derived suppressor cells, have been shown to be associated with an immunosuppressive microenvironment and worse outcomes (31). The M2 subtypes of macrophages have been observed to be stimulated by Th2 cytokines, including IL-4, IL-10 and IL-13. These cells have also been revealed to express CD206 (mannose receptor), arginase 1 and scavenger receptors (32,33). TAMs resemble M2 macrophages by secreting pro-tumor cytokines (such as IL-10, CCL22, VEGF and MMP9) (34), thereby facilitating tumor progression. Kundu *et al* (31) reported a positive association between M2 macrophage infiltration and the malignant progression of BC. Patients with high infiltration levels of M2 macrophages in BC typically have a worse prognosis and have decreased immunotherapeutic sensitivity (35). The present findings indicated that DHX15 expression was positively significant associated with T helper cells, Tcm, and weak positive correlation Th2 cell and M2 macrophage infiltration through ssGSEA and CIBERSORT analyses. Therefore, it is hypothesized that increased DHX15 expression in BC cells may stimulate M2 macrophages by activating Th2 cell infiltration, resulting in worse prognosis and immuno-resistance. The single-cell transcriptomic analysis revealed that DHX15 was highly expressed not only in malignant breast glandular cells but also in T cells and macrophages within the TIME. DHX15 in endometrial carcinoma may promote the secretion of chemotactic factors that recruit immunosuppressive macrophages and T cells (15), which is consistent with the present correlation analysis showing a positive association between DHX15 expression and the infiltration of M2 macrophages and Th2 cells. By contrast, DHX15 is also known to function as a cytosolic nucleic acid sensor in innate immune cells, where it can modulate NF-κB and IFN regulatory factor 3 signaling to influence cytokine production and immune cell polarization (36,37). Therefore, DHX15 expression in T cells and macrophages could directly regulate their functional states, such as promoting M2 macrophage polarization or Th2 cell differentiation, independent of tumor cell-derived signals.

The proportional hazards model analysis indicated that DHX15 functions as an independent prognostic factor in cases where multiple infiltrating immune cell types are present in BC. Kaplan-Meier survival analysis combined with immune infiltration data indicated that the infiltration of $CD8^+$ T cells, $CD4^+$ T cells, neutrophils and dendritic cells was significantly associated with the prognosis of BC, where the group with high DHX15 expression exhibited a worse prognosis. This finding indicates an association between DHX15, immune response and clinical outcomes. Immune checkpoints are crucial for tumor progression, where inhibiting these checkpoints can block cancer cell immune escape (38). In the present study, DHX15 expression was positively associated with Treg markers (FOXP3, CCR8 and STAT5B) and negatively associated with the immune checkpoints PDCD1, LAG3 and GZMB. Collectively, the prognostic effect of DHX15 is tightly intertwined with the TIME. DHX15 correlates positively with Treg signature genes to promote immunosuppression, while it negatively associates with effector immune checkpoint and cytotoxic markers, thereby limiting the antitumor activity of $CD8^+$ T cells and resulting in worse clinical prognosis. Next, DHX15 expression in BC and its biological functions through *in vitro* experiments were determined. Following shRNA-mediated interference of DHX15 expression, BC cells exhibited reduced migration capacity, invasive ability and proliferation levels, whilst overexpressing DHX15 expression increased these cellular functions, further validating the accuracy of prior predictions. This is consistent with the *in vitro* functional data showing that in non-small cell lung cancer, DHX15 serves as an essential mediator of lncRNA-induced invasive phenotypes, while DHX15 upregulation also facilitates metastatic progression in endometrial, colorectal and liver cancers through activation of STAT3/NF-κB axes and metabolic reprogramming (27,39,40). These findings suggest that DHX15 exerts a key biological role in the progression of BC.

The present study also revealed that DHX15 expression was associated with immune cell infiltration in BC tumors through bioinformatics analysis, demonstrating that DHX15 expression may be associated with the TIME and could serve as a basis for future investigation into its role in immunotherapy response.

There were, however, limitations to the present study due to the lack of *in vitro* and *in vivo* assays to validate the effects of DHX15 on BC cell immunity. For future research, the role of DHX15 in regulating BC cell immunity and drug sensitivity through both *in vitro* and *in vivo* experiments should be validated. Whilst the present bioinformatics analysis suggests that DHX15 may be involved in the p53/Rb, WNT and mTOR signaling pathways, the present study did not experimentally validate these predictions. Future studies employing pathway-specific inhibitors, western blot analysis of key signaling components and gene knockdown/rescue experiments are warranted to elucidate the precise molecular mechanisms through which DHX15 promotes BC cell proliferation and migration. Notably, some statistically significant correlations between DHX15 and immune signatures from ssGSEA and CIBERSORT analyses presented correlation coefficients below 0.3, which are defined as weak correlations, and subsequent experimental validation is essential to validate these preliminary bioinformatic observations. The present study served as foundational preclinical work requiring subsequent *in vivo* validation. Future studies should plan to conduct functional co-culture assays or *in vivo* immune profiling following DHX15 modulation and experimentally validate whether these immune-related associations functionally

contribute to the malignant phenotype or to resistance against immunotherapy.

To conclude, the present study employed an integrated approach combining bioinformatics analysis and experiments to investigate the expression of DHX15, its biological function and altered immune cell infiltration patterns in BC. The findings suggest that high expression of DHX15 in BC is associated with a worse prognosis and altered immune cell infiltration patterns. Furthermore, functional assays revealed that DHX15 can promote BC cell proliferation, migration and invasion *in vitro*. Collectively, DHX15 serves as a novel prognostic biomarker and a promoter of malignancy phenotypes in BC; however, the immune-related findings in the present study are purely bioinformatics predictions and await experimental verification in subsequent research.

Acknowledgements

Not applicable.

Funding

The present study was funded by the Tianjin Municipal Education Commission's Scientific Research Plan Project (grant no. 2023KJ043).

Availability of data and materials

The data generated in the present study may be requested from the corresponding author.

Authors' contributions

FL and QY designed and performed the experiments, compiled and analyzed the data and assisted in writing the manuscript. FL also performed the bioinformatics analysis. JL designed the experiments and provided the funding. FL and JL confirm the authenticity of all the raw data. All authors read and approved the final version of the manuscript.

Ethics approval and consent to participate

Not applicable.

Patient consent for publication

Not applicable.

Competing interests

The authors declare that they have no competing interests.

References

1. Siegel RL, Kratzer TB, Giaquinto AN, Sung H and Jemal A: Cancer statistics, 2025. CA J Clin 75: 10-45, 2025.
2. Sung H, Ferlay J, Siegel RL, Laversanne M, Soerjomataram I, Jemal A and Bray F: Global cancer statistics 2020: GLOBOCAN Estimates of incidence and mortality worldwide for 36 cancers in 185 countries. CA Cancer J Clin 71: 209-249, 2021.
3. Bergin ART and Loi S: Triple-negative breast cancer: Recent treatment advances. F1000Res 8: F1000, 2019.
4. Lei S, Zheng R, Zhang S, Chen R, Wang S, Sun K, Zeng H, Wei W and He J: Breast cancer incidence and mortality in women in China: Temporal trends and projections to 2030. Cancer Biol Med 18: 900-909, 2021.
5. Siegel RL, Miller KD and Jemal A: Cancer statistics, 2020. CA J Clin 70: 7-30, 2020.
6. Chen XM, Liang YB, Zuo JX, Yang ZS, Zhang LY, Zhang XY, Wan P and Ke Y: ZG16B: A key regulator of tumor progression and immune microenvironment modulation in cancer (Review). Int J Mol Med 57: 58, 2026.
7. Li Q, Guo H, Xu J, Li X, Wang D, Guo Y, Qing G, Van Vlierberghe P and Liu H: A helicase-independent role of DHX15 promotes MYC stability and acute leukemia cell survival. iScience 27: 108571, 2024.
8. Fan L, Guo X, Zhang J, Wang Y, Wang J and Li Y: Relationship between DHX15 expression and survival in colorectal cancer. Rev Esp Enferm Dig 115: 234-240, 2023.
9. Detanico T, Virgen-Slane R, Steen-Fuentes S, Lin WW, Rhode-Kurnow A, Chappell E, Correa RG, DiCandido MJ, Mbow ML, Li J and Ware CF: Co-expression networks identify DHX15 RNA helicase as a B cell regulatory factor. Front Immunol 10: 2903, 2019.
10. Wang G, Xiao X, Wang Y, Chu X, Dou Y, Minze LJ, Ghobrial RM, Zhang Z and Li XC: The RNA helicase DHX15 is a critical regulator of natural killer-cell homeostasis and functions. Cell Mol Immunol 19: 687-701, 2022.
11. Xu Y, Song Q, Pascal LE, Zhong M, Zhou Y, Zhou J, Deng FM, Huang J and Wang Z: DHX15 is up-regulated in castration-resistant prostate cancer and required for androgen receptor sensitivity to low DHT concentrations. Prostate 79: 657-666, 2019.
12. Xie C, Liao H, Zhang C and Zhang S: Overexpression and clinical relevance of the RNA helicase DHX15 in hepatocellular carcinoma. Hum Pathol 84: 213-220, 2019.
13. Pan L, Li Y, Zhang HY, Zheng Y, Liu XL, Hu Z, Wang Y, Wang J, Cai YH, Liu Q, *et al*: DHX15 is associated with poor prognosis in acute myeloid leukemia (AML) and regulates cell apoptosis via the NF-kB signaling pathway. Oncotarget 8: 89643-89654, 2017.
14. Ito S, Koso H, Sakamoto K and Watanabe S: RNA helicase DHX15 acts as a tumour suppressor in glioma. B J Cancer 117: 1349-1359, 2017.
15. Balaya RD, Kanekar S, Kumar S and Kandasamy RK: Role of DEAD/DEAH-box helicases in immunity, infection and cancers. Cell Commun Signal 23: 292, 2025.
16. Hashemi V, Masjedi A, Hazhir-Karzar B, Tanomand A, Shotorbani SS, Hojjat-Farsangi M, Ghalamfarsa G, Azizi G, Anvari E, Baradaran B and Jadidi-Niaragh F: The role of DEAD-box RNA helicase p68 (DDX5) in the development and treatment of breast cancer. J Cell Physiol 234: 5478-5487, 2019.
17. Li T, Fan J, Wang B, Traugh N, Chen Q, Liu JS, Li B and Liu XS: TIMER: A web server for comprehensive analysis of tumor-infiltrating immune cells. Cancer Res 77: e108-e110, 2017.
18. Chandrashekar DS, Bashel B, Balasubramanya SAH, Creighton CJ, Ponce-Rodriguez I, Chakravarthi BVSK and Varambally S: UALCAN: A portal for facilitating tumor subgroup gene expression and survival analyses. Neoplasia 19: 649-658, 2017.
19. Gyorffy B, Lanczky A, Eklund AC, Denkert C, Budczies J, Li Q and ZSzallasi Z: An online survival analysis tool to rapidly assess the effect of 22,277 genes on breast cancer prognosis using microarray data of 1,809 patients. Breast Cancer Res Treat 123: 725-731, 2010.
20. Fekete JT and Gyorffy B: ROCplot.org: Validating predictive biomarkers of chemotherapy/hormonal therapy/anti-HER2 therapy using transcriptomic data of 3,104 breast cancer patients. Int J Cancer 145: 3140-3151, 2019.
21. Vasaikar SV, Straub P, Wang J and Zhang B: LinkedOmics: Analyzing multi-omics data within and across 32 cancer types. Nucleic Acids Res 46: D956-D963, 2018.
22. Zhou Y, Zhou B, Pache L, Chang M, Khodabakhshi AH, Tanaseichuk O, Benner C and Chanda SK: Metascape provides a biologist-oriented resource for the analysis of systems-level datasets. Nat Commun 10: 1523, 2019.
23. Uhlen M, Fagerberg L, Hallstrom BM, Lindskog C, Oksvold P, Mardinoglu A, Sivertsson A, Kampf C, Sjöstedt E, Asplund A, *et al*: Proteomics. Tissue-based map of the human proteome. Science 347: 1260419, 2015.
24. Yuan H, Yan M, Zhang G, Liu W, Deng C, Liao G, Xu L, Luo T, Yan H, Long Z, *et al*: CancerSEA: A cancer single-cell state atlas. Nucleic Acids Res 47: D900-D908, 2019.

25. Ren T, Wei G, Yi J, Zhang Y, Zhao H, Wu N, Zhang H, Guo Z, Wang Y, Kuang J, *et al*: GPATCH3, a splicing regulator that facilitates tumor immune evasion via the modulation of ATPase activity of DHX15. Front Immunol 16: 1612461, 2025.
26. Jing Y, Nguyen MM, Wang D, Pascal LE, Guo W, Xu Y, Ai J, Deng FM, Masoodi KZ, Yu X, *et al*: DHX15 promotes prostate cancer progression by stimulating Siah2-mediated ubiquitination of androgen receptor. Oncogene 37: 638-650, 2018.
27. Portoles I, Ribera J, Fernandez-Galan E, Lecue E, Casals G, Melgar-Lesmes P, Fernández-Varo G, Boix L, Sanduzzi M, Aishwarya V, *et al*: Identification of Dhx15 as a major regulator of liver development, regeneration, and tumor growth in zebrafish and mice. Int J Mol Sci 25: 3716, 2024.
28. Zheng W, Wang X, Yu Y, Ji C and Fang L: CircRNF10-DHX15 interaction suppressed breast cancer progression by antagonizing DHX15-NF-kappaB p65 positive feedback loop. Cell Mol Biol Lett 28: 34, 2023.
29. Lo YL, Lin HC, Lee Y, Chuang HY and Chou TF: TME-responsive nanoparticles co-targeting VCP, NETs, and dual immune checkpoints for immune revitalization in EGFR/PD-L1/CTLA-4-driven colorectal cancer. Biomed Pharmacother 192: 118565, 2025.
30. Dieci MV, Miglietta F and Guarneri V: Immune infiltrates in breast cancer: Recent updates and clinical implications. Cells 10: 223, 2021.
31. Kundu M, Butti R, Panda VK, Malhotra D, Das S, Mitra T, Kapse P, Gosavi SW and Kundu GC: Modulation of the tumor microenvironment and mechanism of immunotherapy-based drug resistance in breast cancer. Mol Cancer 23: 92, 2024.
32. Sadeghalvad M, Mohammadi-Motlagh HR and Rezaei N: Immune microenvironment in different molecular subtypes of ductal breast carcinoma. Breast Cancer Res Treat 185: 261-279, 2021.
33. Del Alcazar CR, Huh SJ, Ekram MB, Trinh A, Liu LL, Beca F, Zi X, Kwak M, Bergholtz H, Su Y, *et al*: Immune escape in breast cancer during in situ to invasive carcinoma transition. Cancer Discov 7: 1098-1115, 2017.
34. Wang Z, Zhang J, Chen H, Zhang X, Zhang K, Zhang F, Xie Y, Ma H, Pan L, Zhang Q, *et al*: Molecular characterization and prognostic modeling associated with M2-like tumor-associated macrophages in breast cancer: Revealing the immunosuppressive role of DLG3. Front Immunol 16: 1650726, 2025.
35. Zhang L, Gu S, Wang L, Zhao L, Li T, Zhao X and Zhang L: M2 macrophages promote PD-L1 expression in triple-negative breast cancer via secreting CXCL1. Pathol Res Pract 260: 155458, 2024.
36. Ramnani B, Devale T, Manivannan P, Haridas A and Malathi K: DHX15 and Rig-I coordinate apoptosis and innate immune signaling by antiviral RNase L. Viruses 16: 1913, 2024.
37. Mosallanejad K, Sekine Y, Ishikura-Kinoshita S, Kumagai K, Nagano T, Matsuzawa A, Takeda K, Naguro I and Ichijo H: The DEAH-box RNA helicase DHX15 activates NF-kappaB and MAPK signaling downstream of MAVS during antiviral responses. Sci Signal 7: ra40, 2014.
38. Thomas R, Al-Khadairi G and Decock J: Immune checkpoint inhibitors in triple negative breast cancer treatment: Promising future prospects. Front Oncol 10: 600573, 2020.
39. Yao G, Chen K, Qin Y, Niu Y, Zhang X, Xu S, Zhang C, Feng M and Wang K: Long non-coding RNA JHDM1D-AS1 interacts with DHX15 protein to enhance non-small-cell lung cancer growth and metastasis. Mol Ther Nucl Acids 18: 831-840, 2019.
40. Ye L, Jiang G, Sun Y and Li B: ARNTL-mediated INO80-DHX15 axis reprograms the glycolytic metabolism and augments the progression of endometrial carcinoma. Cell Death Dis 16: 463, 2025.